(Preprint) AAS 17-607

SATELLITE CONSTELLATION ORBIT DESIGN TO ENABLE A SPACE-BASED RADIO INTERFEROMETER

Sonia Hernandez*, Jeffrey R. Stuart*, David M. Garza*, Stephen B. Broschart*, Sebastian J. I. Herzig* and Steve A. Chien*

Two different design methods for a networked constellation of N small satellites are presented. In the first method, the (linear) Clohessy-Wilthsire equations are used as an initial design tool, followed by conversion to a two-body model. Discrepancies between the linear and nonlinear solutions are minimized in the conversion process. The second method utilizes invariant manifold theory, by perturbing a reference trajectory in different directions along the center eigenvectors. Both methods require $5N$ parameters to fully define a constellation. In a relative, rotating frame of the reference path, the spacecraft appear as periodic ellipses of varying sizes. Deployment, reconfiguration using propulsive maneuvers, and station keeping costs for an example mission scenario are addressed.

INTRODUCTION

Missions involving multiple, communicating spacecraft have recently gained increased attention due to their potential benefits in reducing cost, increasing robustness, and enabling novel types of missions.[1,2] Such missions are typically referred to as fractionated or (networked) constellation missions. Particularly small form factor spacecraft, such as CubeSats are seen as promising enablers due their low production and launch cost. Also, advancements in autonomy make operations of constellations more manageable and less costly.

Of particular interest to the astronomy science community is the observation of distant objects at frequencies below 30 Mhz. At these wavelengths, a single antenna with a diameter of hundreds of kilometers would be required to gather meaningful data. Therefore, in practice, radio interferometers are used instead. Radio interferometers are radio telescopes consisting of multiple antennas that receive radio waves from the same astronomical object and achieve the same angular resolution as that of a single telescope with the same aperture. However, due to the long baselines (distances between telescopes) required, and due to severe distortions of radio signals at frequencies below 30 Mhz by the ionosphere, Earth-based telescopes are not a good option. One solution is space-based radio interferometers, where a number of low-cost satellites in a (networked) constellation act as an array of radio telescopes and a mothership in a reference orbit can act as a relay for the constellation. Interesting mission scenarios have been proposed such as the observation of coronal mass ejections from the Sun (constellation placed around a geostationary graveyard orbit)[3] and the observation of distant galaxies (constellation placed around a low altitude lunar orbit).[4] Both mission concepts are addressed in the paper as examples for the orbit design.

*Jet Propulsion Laboratory, California Institute of Technology, 4800 Oak Grove Drive, Pasadena, CA 91109. Corresponding Author: Sonia Hernandez; *Tel*: (818) 354-0418; *E-mail address*: Sonia.Hernandez-Doran@jpl.nasa.gov.

How many satellites are needed, where to place them, and in what type of orbit now becomes the mission design challenge. One option is to place the satellites in orbit close to the main gravitational body, so that two-body motion is accurate enough to design the constellation. Moreover, since the constellation must remain close together (constraint given by a maximum allowed baseline), the periods of their orbits must be the same (to avoid drifting away from one another). The design can be therefore accomplished by orbits that vary in eccentricity, inclination, argument of periapsis, and longitude of the node, but have equivalent semi-major axis. In a relative, rotating frame fixed at the mothership, these orbits appear as 2×1 ellipses or "rings" of varying sizes and centers.

Two different methods for constellation design are studied. The first method uses the Clohessy-Wiltshire (CW) equations of motion,[5,6] which linearize the dynamics about a reference spacecraft orbiting in circular motion about the primary body. The CW equations of motion provide an analytical framework, which greatly reduces the complexity in the design, allowing for fast comparison of constellation geometries to obtain the maximum amount of coverage for science purposes. However, because this model assumes linear motion, conversion into nonlinear (more realistic) dynamics must be addressed. The second method uses invariant manifold theory, by exciting the center eigenvectors of the reference path in different directions to create the constellation. This method makes use of the state transition matrix, which, as in the first method, assumes linearization about a reference path for its computation. The main difference with the first method, however, is that the state transition matrix can be computed numerically for any complex dynamical environment (although we restrict the results in this paper to two-body dynamics only). Even though both methods are derived using different approaches, they both methods require $5N$ parameters to fully define a constellation, where N is the total number of spacecraft.

The formation design is driven by adequate coverage of desired mission targets, with coverage defined by the diversity of observations formed by individual spacecraft pairs. In some scenarios, reconfiguration of the constellation can be crucial to obtain the required science data. In this paper we address reconfiguration by thrusting perpendicular to the velocity vector, ensuring that the period of the constellation remain constant. Several investigations have examined the optimization of spacecraft formations for interferometric imaging. For example, active reconfiguration of the formation via optimization is a possible option for covering more targets.[7,8,9] For passively controlled constellations, where reconfiguration is not an option, particle swarm optimization can be used to design the geometry of the formation for maximum baseline coverage.[10,3] In this paper, we do not focus our work on optimization techniques; however, the methods outlined lend themselves well to be optimized if the mission scenario requires it.

The paper is organized as follows. The first section derives the equations of motion for the two constellation design methods. For both methods, step-by-step algorithms are outlined for the user to implement. The second section deals with operations necessary to fly the constellation, such as deployment, reconfiguration, and stationkeeping maneuvers. A lunar radio interferometer mission with thirty-two spacecraft is outlined in the third section, analyzing mission costs as well as coverage. The last section discusses the conclusion and future work.

CONSTELLATION DESIGN METHODS

Any formation design strategy must begin with a method to predict and analyze both the absolute as well as relative motion of the spacecraft. Many methods for formation design have been used in the past, such as perturbations of conic elements,[11] the Clohessy-Wiltshire (CW) equations of relative motion,[5,12] and application of dynamical systems using eigenvalues.[13] Note that for a two-

body dynamical model, all three design strategies can produce equivalent relative motions given the correct assumptions and selection criteria. In this paper we focus on two of the three design strategies. The first method uses the (linear) CW equations of motion. This method provides an analytical framework for fast and simple formation design, which proves useful in the early design stages. Because this model assumes linear motion, conversion into nonlinear (more realistic) dynamics is then outlined. Invariant manifold theory is used as a second option for formation design. This method is especially useful when higher order dynamics want to be considered in the design. The two methods outlined are:

1. Constellation design using Linear Dynamics (CLD)
2. Constellation design using Invariant Manifolds (CIM)

A mothership (reference spacecraft) and N daughter spacecraft orbit a central body, assumed to be spherical with gravitational parameter μ. The mothership orbit is circular, with position and velocity vectors $\mathbf{r}_m$ and $\mathbf{v}_m$, respectively, defined in an inertial frame $I = \{\hat{\mathbf{i}}, \hat{\mathbf{j}}, \hat{\mathbf{k}}\}$. Similarly, daughter i has position and velocity vectors $\mathbf{r}_i$ and $\mathbf{v}_i$, where $i \in \{1, ..., N\}$. The daughters are assumed to orbit nearby the mothership. Relative to the mothership, daughter i has position and velocity vector

$$\begin{aligned} \mathbf{r}_{i/m} &= \left[x_i\, \hat{\mathbf{i}}_\mathbf{r}, y_i\, \hat{\mathbf{i}}_\mathbf{t}, z_i\, \hat{\mathbf{i}}_\mathbf{n}\right]^T \\ \mathbf{v}_{i/m} &= \left[\dot{x}_i\, \hat{\mathbf{i}}_\mathbf{r}, \dot{y}_i\, \hat{\mathbf{i}}_\mathbf{t}, \dot{z}_i\, \hat{\mathbf{i}}_\mathbf{n}\right]^T \end{aligned} \tag{1}$$

where $\hat{\mathbf{i}}_\mathbf{r}$ is a unit vector in the direction of $\mathbf{r}_m$ (*radial*), $\hat{\mathbf{i}}_\mathbf{n}$ is a unit vector perpendicular to the plane of motion of the mothership with respect to the central body (*normal*), and $\hat{\mathbf{i}}_\mathbf{t}$ completes the right handed frame (*transverse* or *in-track*). See Figure 1.

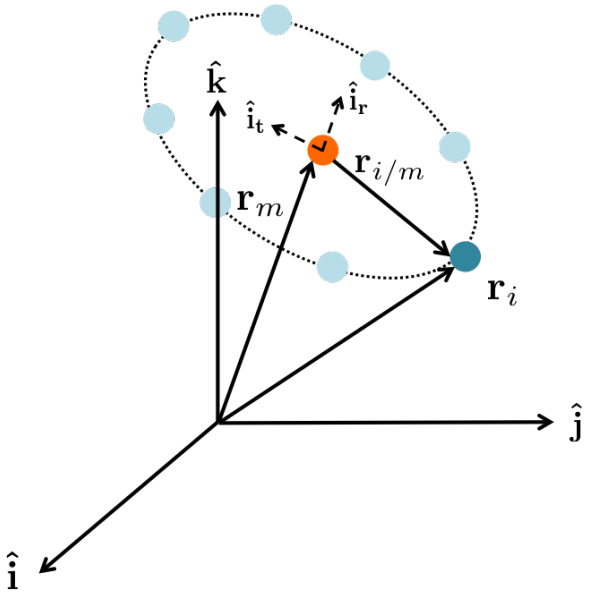

Figure 1. Formation schematic in an inertial frame, where the mothership is in *orange* and in *blue* are the daughter spacecraft.

1. Constellation design using Linear Dynamics

When dealing with formations of many spacecraft, having a fast and simple design method that allows for many trade studies, and is at the same time accurate, is desired. These trade studies are important, not only for the mission design aspect of a mission, but as well for the science team to make sure their objectives are met. For this reason, the Clohessy-Wiltshire equations of relative motion[5] are used. Even though these equations are linear in nature, for formations which remain near the reference orbit, the trajectory resembles that of a nonlinear solution where two-body motion is assumed.

Equations of Motion The equations of motion of daughter i and of the mothership with respect to the central body are

$$\ddot{\mathbf{r}}_i = -\mu \frac{\mathbf{r}_i}{r_i^3} \quad \text{and} \quad \ddot{\mathbf{r}}_m = -\mu \frac{\mathbf{r}_m}{r_m^3} \tag{2}$$

where no external perturbations are assumed to act on either spacecraft. Using relative motion equations, the acceleration of daughter i can also be written as

$$\ddot{\mathbf{r}}_i = \ddot{\mathbf{r}}_m + \ddot{\mathbf{r}}_{i/m} + 2\boldsymbol{\omega} \times \dot{\mathbf{r}}_{i/m} + \boldsymbol{\omega} \times \boldsymbol{\omega} \times \mathbf{r}_{i/m} \tag{3}$$

where $\boldsymbol{\omega}$ is the mean motion of the mothership: $\boldsymbol{\omega} = \omega \hat{\mathbf{i}}_{\mathbf{n}}$ and $\omega = \sqrt{\mu / r_m^3}$. Note $\boldsymbol{\omega}$ is constant since the motion of the mothership is assumed to be circular around the central body.

Solving for $\ddot{\mathbf{r}}_{i/m}$ in Eq. (3), the acceleration of daughter i with respect to the mother spacecraft is

$$\ddot{\mathbf{r}}_{i/m} = \ddot{\mathbf{r}}_i - \ddot{\mathbf{r}}_m - 2\omega \begin{bmatrix} -\dot{y}_i \\ \dot{x}_i \\ 0 \end{bmatrix} + \omega^2 \begin{bmatrix} x_i \\ y_i \\ 0 \end{bmatrix} \tag{4}$$

where $(\ddot{\mathbf{r}}_i - \ddot{\mathbf{r}}_m)$ in Eq. (4) can be approximated by, first, using a binomial expansion to first order, and, secondly, assumming that $\mathbf{r}_{i/m}$ is small and, therefore, powered terms are negligible:

$$\begin{aligned} \ddot{\mathbf{r}}_i - \ddot{\mathbf{r}}_m &= -\frac{\mu}{r_m^3} \left(\mathbf{r}_m - r_m^3 \frac{\mathbf{r}_i}{r_i} \right) \\ &\approx -\frac{\mu}{r_m^3} \left(\mathbf{r}_{i/m} - \frac{3}{r_m^2} (\mathbf{r}_m \cdot \mathbf{r}_{i/m}) \mathbf{r}_m \right) \\ &= -\omega^2 \begin{bmatrix} -2x_i \\ y_i \\ z_i \end{bmatrix} \end{aligned} \tag{5}$$

Plugging Eq. (5) into Eq. (4), the relative, *linear* equations of motion of daughter i with respect to the mother are

$$\begin{aligned} \ddot{x}_i &= 2\omega \dot{y}_i + 3\omega^2 x_i \\ \ddot{y}_i &= -2\omega \dot{x}_i \\ \ddot{z}_i &= -\omega^2 z_i \end{aligned} \tag{6}$$

Note that the motion of the out-of-plane component z_i is a decoupled harmonic oscillator, and is independent of the in-plane motion.

Table 1. Ring formation definition parameters using CLD

Formation Parameters	Ring Parameters	
	In-plane	Out-of-plane
ω = orbit period	A = ring size	B = max. displacement
n_r = n° rings	ϕ = angular displacement	β = ring orientation
$n_{sc/r}$ = n° of spacecraft/ring	y_c = center of ring	

An analytical solution to Eq. (6) exists and is given by[14]

$$\begin{aligned} x_i(t) &= 2\left(2x_{i_0} + \dot{y}_{i_0}/\omega\right) - \left(3x_{i_0} + 2\dot{y}_{i_0}/\omega\right)\cos\xi + \left(\dot{x}_{i_0}/\omega\right)\sin\xi \\ y_i(t) &= \left(y_{i_0} - 2\dot{x}_{i_0}/\omega\right) - 3(2x_{i_0} + \dot{y}_{i_0}/\omega)\xi + (2\dot{x}_{i_0}/\omega)\cos\xi + 2(3x_{i_0} + 2\dot{y}_{i_0}/\omega)\sin\xi \\ z_i(t) &= z_{i_0}\cos\xi + (\dot{z}_{i_0}/\omega)\sin\xi \end{aligned} \quad (7)$$

where $\xi = \omega t$ and the initial conditions at time t_0 are given by x_{i_0}, y_{i_0}, and z_{i_0} in position and $\dot{x}_{i_0}$, $\dot{y}_{i_0}$, and $\dot{z}_{i_0}$ in velocity. For periodic motion, the secular term in Eq. (7) must vanish, i.e.

$$2x_{i_0} + \dot{y}_{i_0}/\omega = 0,$$

leading to

$$\begin{aligned} x_i(t) &= \frac{1}{2}A\sin(\alpha + \phi_i(t)) \\ y_i(t) &= A\cos(\alpha + \phi_i(t)) + y_c \\ z_i(t) &= B\sin(\beta + \phi_i(t)) \end{aligned} \quad (8)$$

where A, B, α, β, and y_c are constants of motion and $\phi_i(t) = \phi_{i_0} + wt$ with ϕ_{i_0} as the initial angular displacement. Without loss of generality, the angular offset constant $\alpha = 0^\circ$ for the remainder of the paper, since the desired angular displacement can be achieved via $\phi_i(t)$. Note that the in-plane motion ($x - y$ plane) is given by a 2×1 ellipse (or *ring*) of semi-major axis size A with center at y_c

$$\left(2x_i(t)\right)^2 + \left(y_i(t) - y_c\right)^2 = A^2,$$

whereas the out-of-plane motion (z axis) is completely decoupled, and has an amplitude of B. The five constants of motion, which are used to define the geometry of a ring are shown in Table 1 under 'Ring Parameters', and a schematic in the relative frame of the mothership is shown in Figure 2. In this frame, the central body is on the far left side of the $\hat{\mathbf{i}}_r$ axis. The term β, not shown in Figure 2, represents the ring orientation, and is similar geometrically to the right ascension of the ascending node. The true anomaly ν_i is offset by 90° from ϕ_i. Therefore, periapsis/apoapsis occurs on the left/right side of the mothership on the $\hat{\mathbf{i}}_r$ axis, and the maximum deviation from the mothership typically occurs at $\nu_i = \pm 90^{\circ *}$. The full analytical state of daughter i in Eq. (1) has position coordinates shown in Eq. (8) and the velocity coordinates are found by taking the time derivative of the position.

*As eccentricity becomes larger, i.e. A grows, the relative orbit transitions from a ring into a kidney-bean shape, typical of Lyapunov orbits in the restricted three-body problem. The maximum deviation from the mothership then will occur after (before) $\nu_i = 90^\circ$ (-90°).

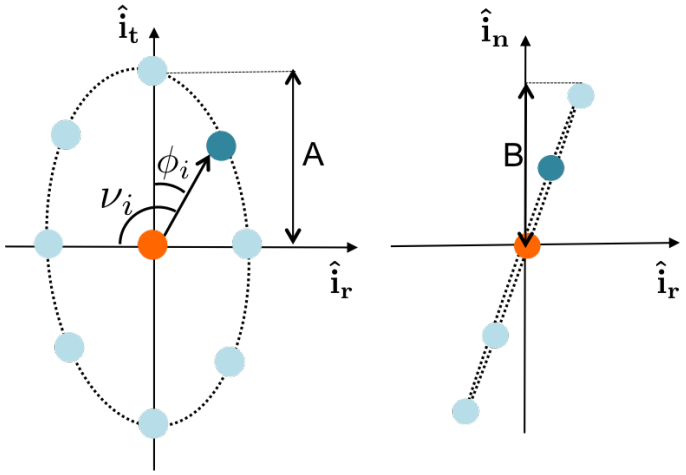

Figure 2. Formation schematic in a relative, rotating frame of the mothership, where the mothership is in *orange* and in *blue* are the daughter spacecraft.

Formation Design A single ring formation can be designed via the parameters shown in Table 1. Depending on the science requirements, several spacecraft can be placed on the designed ring, with a specific initial angular displacement. Placing the daughters on several rings n_r of different size, may allow for more science acquisition, depending on the mission at hand. The algorithm to design such type of constellation is shown in Table 2. The beauty of this method is that the design is analytical, and therefore, no integration is required, making it of great use for initial design searches.

Table 2. Algorithm for Constellation design using Linear Dynamics (CLD)

1:	**Input** mothership parameters: $\mathbf{r}_{m_0}$, $\mathbf{v}_{m_0}$, μ
2:	Compute $r_{m_0} = \lvert\mathbf{r}_{m_0}\rvert$, $v_{m_0} = \lvert\mathbf{v}_{m_0}\rvert$, $a_m = 1/\left(2/r_{m_0} - v_{m_0}^2\right)$, and $\omega = \sqrt{\mu/a_m^3}$
3:	**Input** formation parameters: n_r, $n_{sc/r}$
	Define ring: for $i = 1, ..., n_r$ input A_i, B_i, y_{c_i}, β_i
	Define spacecraft phase: for $j = 1, ..., n_{sc/r}$ input ϕ_{i_j}
4:	Compute total n° of s/c: $N = n_r n_{sc/r}$
5:	Compute $\mathbf{r}_{i/m}$, $\mathbf{v}_{i/m}$ for $i = 1, ..., N$ from Eq. (8) and $\frac{d}{dt}$(Eq. (8))
6:	**Output**: $\mathbf{r}_{i/m}$, $\mathbf{v}_{i/m}$ for $i \in (1, ..., N)$

Using the CLD algorithm, a constellation for an example interferometry mission is designed and shown in Figure 3. The constellation design includes a mothership spacecraft in a circular, $5,000$ km orbit about the Moon ($\mu = 4,903$ km^3/s^2), and 30 daughterships orbiting the mothership in a nearby cluster. For this particular example, the mothership orbit was chosen for science purposes to be far enough from the Earth to avoid interference, as well as minimize gravitational perturbations from Earth. By using the algorithm in Table 2, the orbits of all the spacecraft are designed to have the same period as the mothership (roughly 8.8 hours), with slightly varying eccentricity and inclination. The maximum allowed baseline between any two spacecraft for science is 600 km (which dictates the maximum value of A). In a relative, rotating frame fixed at the mothership, the equal period orbits are accomplished by the ring shaped orbits of varying sizes and centers, mimicking a gear-like movement which allows for optimum baseline coverage (Figure 3(b)).

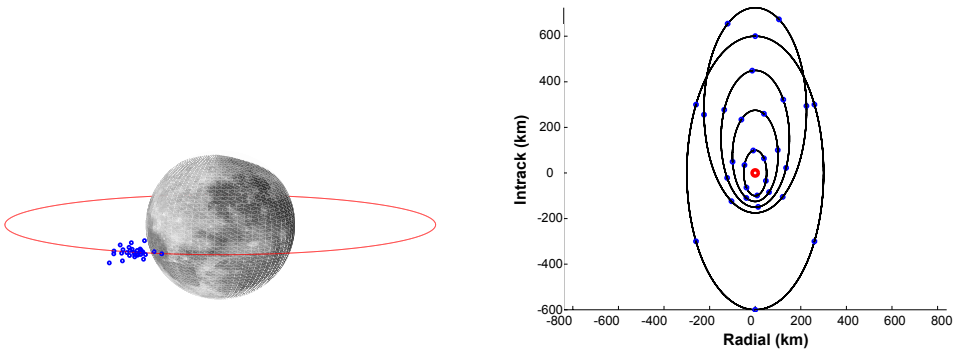

(a) Inertial, Fixed Frame

(b) Relative, Rotating Mothership Frame

Figure 3. CLD of mothership and daughter spacecraft orbiting the Moon, where the mothership is in a $5,000$ km circular, equatorial orbit.

Converting from Mothership-Relative Frame to a Fixed-Inertial Frame The position and velocity vectors of daughter i with respect to a rotating frame fixed at the mothership, $\mathbf{r}_{i/m}$ and $\mathbf{v}_{i/m}$, can be transformed to an inertial, fixed frame with the transformation shown below. Assuming the state of the mothership is known at some point in time t, the position and velocity of the daughter is:

$$\begin{aligned} \mathbf{r}_i &= \mathbf{r}_m + R_3(\theta)\mathbf{r}_{i/m} \\ \mathbf{v}_i &= \mathbf{v}_m + R_3(\theta)\mathbf{v}_{i/m} + \dot{R}_3(\theta)\mathbf{r}_{i/m} \end{aligned} \tag{9}$$

where $R_3(\theta)$ is a z-axis rotation and $\dot{R}_3(\theta)$ its time-derivative, with $\theta = (2\pi/T_p)t$ and $T_p = 2\pi/\omega$. The conversion from relative to inertial frame can readily be done by taking the inverse of Eq. (9).

Converting From Linear to Nonlinear Motion The equations in (8) are useful for initial design, due to their simplicity in the formation definition. However, linear motion only follows nonlinear motion for small displacements from the mothership. An example is shown in Figure 4(a), where the same initial conditions are used to propagate the state of a daughter using linear equations of motion (Eq. 6) versus the nonlinear equations of motion (Eq. 2), with ring parameters defined in Table 3. Since periodic motion is a requirement for the formation design, the nonlinear state must be corrected to exhibit this type of behavior.

We begin by converting the daughter initial conditions $\mathbf{r}_i$ and $\mathbf{v}_i$ into keplerian orbital elements. At this point, the semi-major axis of daughter i, a_i, is not equivalent to that of the mothership, a_m. To find periodicity of the orbit, we change the initial daughter state by forcing the semi-major axis $a_i^* = a_m$. The goal, however, is to find periodicity *while* ensuring the discrepancies between the initial (linear) ring design and the converted nonlinear design are minimized.

Depending on where along the orbit we choose to correct the period, the ring in nonlinear dynamics will behave differently. This can be seen in Figure 4(b), in the *blue* trajectories, which is showing the corrected ring solutions with initial phase angle $0 \leq \phi_0 < 360^o$. The closest ring formation in nonlinear dynamics to the linear one is the *cyan* colored trajectory, at $\phi_0 = 0^o$, which corresponds to the apsis of the ring ($\phi_0 = 180^o$ gives the same solution). Even though only one example is shown, many test cases show that converting to a nonlinear model at $\phi_0 = 0^\circ$ results in the minimum deviation from the linear model. The initial location of the spacecraft (cyan and red dots)

have been shifted in phase, which is equivalent to a timing offset. This behavior is easily corrected by shifting the initial phase (or true anomaly ν_i) of the daughter to the desired one. The algorithm to distribute the constellation using nonlinear dynamics is described in Table 4. As in CLD, $5N$ parameters are required to generate the constellation: $4N$ ring geometry parameters and N phasing offsets. Note that the phasing offset is now defined by ν_i rather than ϕ_i, where $\nu_i = \phi_i - 90°$.

Table 3. Ring parameters for the example in Figure 4, with $\mu = 4,903$ km^3/s^2 and $a_m = 5,000$ km

$A = 600$ km	$B = 0$ km	$y_c = 0$ km	$\alpha = 0°$	$\beta = 0°$

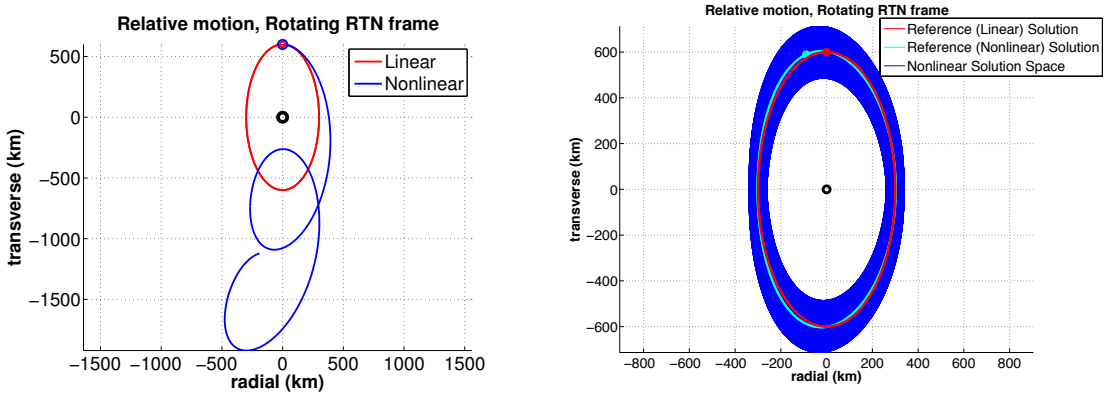

(a) Non-corrected Nonlinear Trajectory

(b) Corrected Nonlinear Trajectory

Figure 4. Linear versus nonlinear trajectories in relative, rotating frame

Table 4. Algorithm for CLD to Nonlinear dynamics

1:	**Input** mothership parameters: $\mathbf{r}_{m_0}$, $\mathbf{v}_{m_0}$, μ
2:	Compute $r_{m_0} = \lvert\mathbf{r}_{m_0}\rvert$, $v_{m_0} = \lvert\mathbf{v}_{m_0}\rvert$, $a_m = 1/\left(2/r_{m_0} - v_{m_0}^2\right)$, and $\omega = \sqrt{\mu/a_m^3}$
3:	Compute $\mathbf{r}_m$, $\mathbf{v}_m$ from $[t_0, T_p]$, where $Tp = 2\pi/\omega$ by propagating Eq. (2)
3:	**Input** formation parameters: n_r, $n_{sc/r}$
	Define ring: for $i = 1, ..., n_r$ input A_i, B_i, y_{c_i}, β_i. Set $\phi_i = 0$
	Define spacecraft phase: for $j = 1, ..., n_{sc/r}$ input ν_{i_j} (true anomaly)
4:	Nonlinear ring geometry for $i = 1, ..., n_r$:
	Compute $\mathbf{r}_{i/m}(t_0)$, $\mathbf{v}_{i/m}(t_0)$ from Eq. (8) and $\frac{d}{dt}$(Eq. (8))
	Compute $\mathbf{r}_i(t_0)$, $\mathbf{v}_i(t_0)$ from Eq. (9)
	Compute orbital elements and change period by $a_i^* = a_m$
	Propagate corrected state using Eq. (2) to obtain $\mathbf{r}_i^*$, $\mathbf{v}_i^*$ from $[t_0, T_p]$
5:	Distribute spacecraft into their respective rings.
	For $i = 1, ..., n_r$
	For $j = 1, ..., n_{sc/r}$
	Solve for t_{i_j} given ν_{i_j} (Kepler's equation)
	Re-initialize: $\mathbf{r}_k^*(t_0) = \mathbf{r}_i(t_{i_j})$, $\mathbf{v}_k^*(t_0) = \mathbf{v}_i(t_{i_j})$, where $k = (i-1) * n_{sc/r} + j$
	Propagate using Eq. (2)
6:	**Ouput** $\mathbf{r}_k^*$, $\mathbf{v}_k^*$ for $k \in (1, ..., N)$

2. Constellation design using Invariant Manifolds

Similar to CLD, the underlying basis for CIM is the linearization of motion around a reference (mothership) spacecraft, assumed to orbit in periodic, circular motion about a central body*, with inertial state vector $\mathbf{X}_m = \left[\mathbf{r}_m^T, \mathbf{v}_m^T\right]^T$.The Keplerian equations of motion in Eq. (2), can also be written in terms of a potential function U,

$$\ddot{\boldsymbol{r}}_m = \frac{\partial U}{\partial \boldsymbol{r}_m} \tag{10}$$

where

$$U = \frac{\mu}{r_m}$$

and $r_m = \|\mathbf{r}_m\|$. For mathematical convenience, we non-dimensionalize the equations of motion by μ and the radius of the central body, R, resulting in the characteristic time $t^* = \sqrt{\frac{R^3}{\mu}}$ and the new potential function $U = 1/r_m$.

The inertial state of a daughter spacecraft orbiting nearby the mothership is $\mathbf{X}_i = \left[\mathbf{r}_i^T, \mathbf{v}_i^T\right]^T$. The motion of daughter i relative to the reference path can be linearized as

$$\dot{\boldsymbol{x}}_i = \boldsymbol{A}(t)\boldsymbol{x}_i \tag{11}$$

where higher order terms of a Taylor expansion are truncated. The relative state vector $\boldsymbol{x}_i = [x_i, y_i, z_i, \dot{x}_i, \dot{y}_i, \dot{z}_i]^T$ and the time-varying linearized dynamic matrix is

$$\boldsymbol{A}(t) = \begin{bmatrix} \mathbf{0}_{3\times3} & \boldsymbol{I}_{3\times3} \\ \frac{\partial^2 U}{\partial \boldsymbol{r}_m^2} & \mathbf{0}_{3\times3} \end{bmatrix} \tag{12}$$

Propagating this linearized motion along a trajectory results in the state transition matrix (STM), $\boldsymbol{\Phi}(t, t_0)$, which maps variations in the initial state to changes in the current state via

$$\boldsymbol{x}_i(t) = \boldsymbol{\Phi}(t, t_0)\boldsymbol{x}_i(t_0) \tag{13}$$

with the change in STM given by

$$\dot{\boldsymbol{\Phi}}(t, t_0) = \boldsymbol{A}(t)\boldsymbol{\Phi}(t, t_0) \tag{14}$$

and initial conditions $\boldsymbol{\Phi}(t_0, t_0) = \boldsymbol{I}_{6\times6}$. When the STM is propagated for one period of a closed orbit (i.e., $\boldsymbol{\Phi}(T + t_0, t_0)$), it is known as the monodromy matrix. Note that Eqs. (11), (13), and (14) are general dynamical equations valid for any model of orbital motion and Eq. (12) is only altered when the equations of motion are also velocity dependent, for example if they are expressed in a rotating frame.

The STM maps differences in the initial conditions along the resulting perturbed paths and contains information about the underlying dynamical system. In particular, the monodromy matrix reveals the fundamental *relative motions* of the associated periodic orbit. The eigenvalues λ_k, $k \in (1, ..., 6)$, of the monodromy matrix indicate the stability of the orbit while the associated eigenvectors $\hat{\mathbf{e}}_k$ can be used to selectively excite the corresponding relative motion. For example,

*Higher-order relative motion can also be captured using this method, but for purposes of this paper, we focus on linearized relative motion.

an eigenvalue with magnitude $\|\lambda_k\| > 1$ denotes unstable motion; perturbing the initial state of the reference periodic orbit by the step ε in the corresponding eigenvector direction establishes an asymptotic departure from the periodic orbit along the unstable manifold. Variations in the orbital initial conditions of daughter spacecraft i due to exciting eigenvalue/eigenvector pairs are expressed as

$$\boldsymbol{X}_i(\tau) = \boldsymbol{X}_m(\tau) + \boldsymbol{x}_i(\tau, \boldsymbol{\theta}_i, \boldsymbol{\varepsilon}_i) \tag{15}$$

where τ is a time-like parameter specifying location on the periodic orbit and $\boldsymbol{x}_i$ is a step into the invariant manifold space. The manifold step for a single eigenvector k is[15]

$$\boldsymbol{x}_i(\tau, \theta_{i_k}, \varepsilon_{i_k}) = \varepsilon_{i_k}\Big(\cos(\theta_{i_k})\mathrm{Re}[\hat{\mathbf{e}}_k(\tau)] - \sin(\theta_{i_k})\mathrm{Im}[\hat{\mathbf{e}}_k(\tau)]\Big)$$

where ε_{i_k} is the step magnitude, θ_{i_k} is an angular parameter, and Re and Im denote the real and imaginary components of the complex vector, respectively.* By convention, we allow ε_{i_k} to encompass both negative and positive values while we restrict θ_{i_k} to fall in the interval $[0°, 180°)$.† We now generalize the mathematical basis of the manifold step to allow linear combinations of the eigenvectors, that is:

$$\boldsymbol{x}_i(\tau, \boldsymbol{\theta}_i, \boldsymbol{\varepsilon}_i) = \sum_{k=1}^{n} \varepsilon_{i_k}\Big(\cos(\theta_{i_k})\mathrm{Re}[\hat{\mathbf{e}}_k(\tau)] - \sin(\theta_{i_k})\mathrm{Im}[\hat{\mathbf{e}}_k(\tau)]\Big). \tag{16}$$

Using this formulation, we can selectively excite or suppress components of the local natural flow relative to a baseline orbit, leading to intricate combined manifold motion.

For any orbit in two-body motion, $\|\lambda_k\| = 1$ for all six eigenvalues, indicating dynamical stability and the presence of a multi-dimensional center manifold, or invariant torus.[15] However, of the six eigenvectors, two form a complex conjugate pair and another two are repeated strictly real vectors, this latter phenomenon indicating that the monodromy matrix is degenerate; the remaining two eigenvectors are unique and strictly real. Thus, we can rewrite Eq. (16) as

$$\boldsymbol{x}_i(\boldsymbol{\varepsilon}_i, \boldsymbol{\theta}_i) = \varepsilon_{i_1}\hat{\mathbf{e}}_1 + \varepsilon_{i_2}\hat{\mathbf{e}}_2 + \varepsilon_{i_3}\hat{\mathbf{e}}_3 + \varepsilon_{i_4}\Big(\cos(\theta_{i_4})\mathrm{Re}[\hat{\mathbf{e}}_4] - \sin(\theta_{i_4})\mathrm{Im}[\hat{\mathbf{e}}_4]\Big) \tag{17}$$

while still retaining the ability to fully exploit the invariant manifold space. Note that we have omitted τ, since we can arbitrarily select a value for τ while still capturing all possible relative formations: our underlying motion is Keplerian and any perturbation at a specific location on the periodic orbit results in perfectly periodic orbits that can be equally realized from any other location on the reference trajectory.

Inspecting Eq. (17), we are required to specify only 5 parameters, $[\varepsilon_{i_1}, \varepsilon_{i_2}, \varepsilon_{i_3}, \varepsilon_{i_4}, \theta_{i_4}]^T$, to generate the 6-element vector defining the initial condition of any daughter spacecraft i; regardless of the manifold step taken, some fundamental characteristic of the baseline periodic orbit is preserved. This conserved quantity is the orbital energy, meaning that any perturbed orbit we specify using CIM will have the same period as our baseline trajectory; thus, using CIM has the additional advantage of automatically preserving our desired passive clustering of the spacecraft.‡ Therefore, to

*When the eigenvector is fully real, that is, $\mathrm{Im}[\hat{\mathbf{e}}_k(\tau)] = \mathbf{0}$, the angular parameter θ_{i_k} can be set to zero without loss of generality.

†It is mathematically equivalent to allow $\theta_{i_k} \in [0°, 360°)$ while restricting ε_{i_k} to strictly non-negative values.

‡This behavior is not unique to our particular orbit: the monodromy matrix of any periodic orbit will be deficient, leading to the preservation of an energy-like parameter (energy for two-body orbits, Jacobi constant for restricted three-body orbits, etc.). Bounded motion will not necessarily be preserved for unstable orbits, but the energy-like value will be.

initialize an N-spacecraft constellation, we need only select values for $5N$ initialization parameters, that is, $4N$ step magnitudes and N angular offsets. Table 5 outlines the algorithm to generate a constellation of N spacecraft using CIM.

Table 5. Algorithm for Constellation design using Invariant Manifolds (CIM)

1:	**Input** mothership parameters: $\mathbf{X}_{m_0}$, μ
2:	Integrate Eq. (10) and (14) to find $\mathbf{X}_m(t)$ and $\mathbf{\Phi}(t, t_0)$ for $t \in [t_0, T + t_0]$
3:	Compute λ_k and $\hat{\mathbf{e}}_k$ for $k = 1, ..., 6$ of the monodromy matrix $\mathbf{\Phi}(T + t_0, t_0)$
4:	**Input** Formation parameters: n_r, $n_{sc/r}$, $N = n_r n_{sc/r}$
	Define ring: for $i = 1, ..., n_r$ input ε_{i_1}, ε_{i_2}, ε_{i_3}, ε_{i_4}
	Define spacecraft phase: for $j = 1, ..., n_{sc/r}$ input $\theta_{i_{j_4}}$
5:	For $i \in (1, ..., N)$:
	Compute $\mathbf{x}_i(t_0)$ from Eq. (17)
	Compute $\mathbf{X}_i(t_0)$ from Eq. (15)
	Propagate to obtain $\mathbf{X}_i(t)$ for $t \in (t_0, t_0 + T)$
6:	**Ouput** $\mathbf{r}_i$, $\mathbf{v}_i$ for $i \in (1, ..., N)$

Example: Constellation around a GEO Graveyard Orbit GEO graveyard orbits operate in a relatively benign environment, and therefore, short-term motion of the satellites is adequately described using Keplerian motion. For this example we use a circular, 25 hour period, equatorial orbit, with $\tau = 0$, the location on the orbit corresponding to $\boldsymbol{X}_m(t_0) = [43,399 \text{ km}, 0, 0, 0, 3.0306 \text{ km/s}, 0]^T$. A constellation of six spacecraft is designed.

Before designing the constellation, we wish to gain some insight into the invariant natural flow and test the potential for human intuition in this complex design space. We begin by assessing the behavior exhibited by each eigenvector, as illustrated in Figure 5, where the circles indicate the start of propagation, diamonds $1/4$, triangles $1/2$, and squares $3/4$ of the orbit. Rather than the traditional

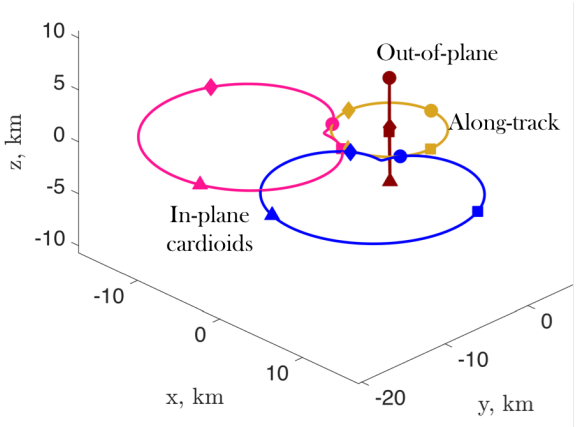

Figure 5. Relative motion arising from exciting individual eigenvectors of the monodromy matrix, shown in axes parallel to equatorial inertial frame axes, centered on the GEO graveyard orbit.

radial, transverse, normal RTN-frame, we use a set of axes $(\hat{x}, \hat{y}, \hat{z})$ parallel to an inertial, Earth-centered frame, with $\hat{x}$ and $\hat{y}$ in the equatorial plane of Earth, but centered on the GEO graveyard orbit. Two motions are readily identifiable as along-track motion associated with the degenerate

repeated eigenvector $\hat{\mathbf{e}}_1$ and out-of-plane motion represented by the complex eigenvector $\hat{\mathbf{e}}_4$. The two in-plane motions linked to the strictly real, unique eigenvectors $\hat{\mathbf{e}}_2$ and $\hat{\mathbf{e}}_3$ exhibit cardioid relative motion in the quasi-inertial frame. Note that we have generated these relative motions by taking positive steps ε_i; using negative values would produce mirror images across the relevant lines of symmetry. Even this brief inspection reveals behaviors of interest: using the along-track eigenvector produces the planar 'ring' formation, while combining the out-of-plane and along-track motions yields elliptical relative motion in the inertially directed axes.

Table 6. Constellation parameters using CIM for 6 spacecraft in a GEO graveyard orbit.

i	ϵ_{i_1} (km)	ϵ_{i_2} (km)	ϵ_{i_3} (km)	ϵ_{i_4} (km)	θ_{i_4} (deg)
1	3	0	-2	2.5	150
2	0	2	-2	2	240
3	-2.5	2	0	3	60
4	-2	0	2.5	3	180
5	0	-2	2	2	300
6	3	-2.5	0	3	120

Using the knowledge gained from Figure 5, a six spacecraft constellation is designed around the GEO graveyard reference orbit, and is shown in Figure 6 with parameters in Table 6. The closest spacecraft-spacecraft approach over the course of the 25-hour period is 3.25-km, while the furthest spacecraft-spacecraft recession is 15-km and the maximum relative velocity is 0.75-m/s. A metric to evaluate the performance of this, or any designed constellation, is explained in the last section of the paper in reference to an example mission scenario.

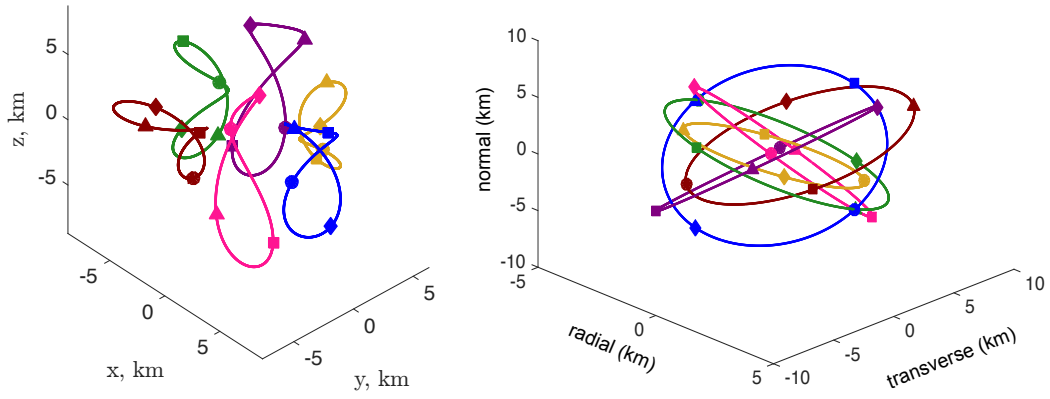

(a) Inertial axes centered on mothership (b) RTN axes centered on mothership

Figure 6. Example six spacecraft constellation generated using CIM algorithm.

CIM and CLD both require $5N$ parameters to define a constellation. Therefore, the same constellation designed using CIM parameters, shown in Figure 6, could have been designed using CLD. Even though both methods are derived using different approaches they can lead to the same design. For the remainder of the paper we will use CLD to address operations in constellations.

FORMATION OPERATIONS

Once a desired formation configuration has been established, our next step is to assess the operational performance of this design. The underlying questions to answer are: how the spacecraft are deployed into their respective orbits; how the constellation can reconfigure to obtain more science data; and how does the passive cluster evolve in the presence of perturbing forces and how often are stationkeeping maneuvers necessary.

Deployment

We assume the daughter spacecraft deploy from the mothership location into the constellation geometry once the mothership reaches its final orbit. For an initial ΔV estimate, a Lambert targeter is used for each spacecraft in the constellation. The transfer time for each daughter into its final configuration is allowed to vary in order to optimize the ΔV. The state of the daughters at time t_0 is known, $\mathbf{X}_m(t_0) = \mathbf{X}_i(t_0)$ for $i = 1, ..., N$. The final relative configuration of the constellation is also known, which is to be reached at some maximum final time $t_{f_{max}}$. By grid searching over time $t_0 \leq t \leq t_{f_{max}}$, the optimal ΔV transfer is found for each daughter. An example of deployment of six spacecraft is shown in Figure 7, (a) at initial deployment time, (b) midway through the reconfiguration, and (c) in the final configuration at $t_{f_{max}}$. The constellation was designed using the CLD to nonlinear algorithm, with parameters in Table 7. The optimized trajectory in the relative frame is very similar for the spacecraft, showing that it is optimal to arrive at the ring at its apogee. The transfer time for each spacecraft, however, is different in order reach the relative desired spacing.

Table 7. Ring parameters for the example in Figure 7 with $\mu = 4,903$ km^3/s^2 and $a_m = 5,000$ km

$A = 300$ km	$B = 0$ km	$y_c = 0$ km	$\beta = 0^\circ$	$\phi_i = [0, 60, 120, 180, 240, 300]^\circ$

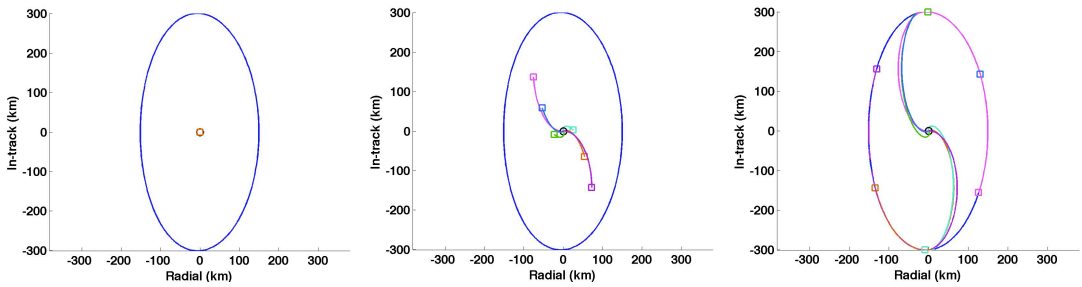

(a) Initial configuration (b) Midway configuration (c) Final configuration

Figure 7. Deployment of six spacecraft from the mothership into a ring.

Reconfiguration

Since the period of the constellation is constant using the design methods in this paper, after one full revolution around the central body, the spacecraft all return to the initial relative configuration. Most of the science and data downlink can be accomplished within a few spacecraft orbits around the central body for a specific configuration. In order to gather more science data, each of the spacecraft on a ring can be reconfigured to change its size, which allows for new relative positioning between

the cluster. The main constraint is to maintain the same orbit period for all spacecraft, which can be accomplished *only* via a maneuver perpendicular to the velocity direction.

Suppose that Eq. (2) is augmented to allow for external perturbations due to a finite thrust engine, with constant magnitude T. The equations of motion are

$$\ddot{\mathbf{r}}_i = -\mu \frac{\mathbf{r}_i}{r_i^3} + \mathbf{f}_i \tag{18}$$

where $\mathbf{f}_i$ is the external acceleration, with magnitude $\|\mathbf{f}_i\| = T/m_i$, m_i is the mass of daughter i which varies according to $\dot{m}_i = -T/c$, where $c = gI_{sp}$, $g = 9.81$ m/s^2, and I_{sp} is the specific impulse of the engine. The energy E_i of a spacecraft under such motion is

$$E_i = \frac{1}{2}(\mathbf{v}_i^T \mathbf{v}_i) - \mu(\mathbf{r}_i^T \mathbf{r}_i)^{-1/2} \tag{19}$$

and its time-derivative under the acceleration in Eq. (18) is

$$\dot{E}_i = \mathbf{v}_i^T \mathbf{f}_i = 0 \Longleftrightarrow \mathbf{f}_i \perp \mathbf{v}_i \tag{20}$$

Therefore, as long as the thrust is perpendicular to the velocity, the energy (or period) of the orbit will remain constant.

The in-plane size of the ellipse A_i is changed by thrusting in the direction $\hat{\mathbf{v}}_i \times \hat{\mathbf{h}}_i$, where $\mathbf{h}_i$ is the angular momentum; whereas the out-of-plane size of the ellipse B_i is changed by thrusting in $\hat{\mathbf{h}}_i$. We define the thrust as

$$\mathbf{f}_i = \frac{T}{m}\left[\frac{k_1 \hat{\mathbf{v}}_i \times \hat{\mathbf{h}}_i + k_2 \hat{\mathbf{h}}_i}{\|k_1 \hat{\mathbf{v}}_i \times \hat{\mathbf{h}}_i + k_2 \hat{\mathbf{h}}_i\|}\right] \tag{21}$$

where k_1 and k_2 are scalars representing the amount of in-plane versus out-of-plane thrust applied.

A schematic example of thrusting only in the radial-intrack plane is shown in Figure 8. The spacecraft begins at t_0, where it performs several revs, until its desired science objectives are met. At time t_1, which corresponds to a true anomaly $\nu_i = -90^\circ$, the spacecraft thrusts to increase it's ring size. Note that by doing so, the ring is not centered anymore at the origin, i.e. $y_c \neq 0$. After the science requirements are met again, the spacecraft thrusts again at t_2, corresponding to $\nu = 90^\circ$, increasing its ring size again, and recentering the ring at the origin. The thrusting can be performed at any point along the orbit, however, thrusting at $\nu_i = \pm 90^\circ$ allows to keep the symmetry of the ring, as well as avoid collisions when multiple rings are present, allowing for a simple solution for the reconfiguration problem.

Figure 9 shows four spacecraft orbiting a mothership, which is in a circular orbit around the Moon at $a_m = 5,000$ km. The initial location of each daughter is shown in a diamond shape in the innermost ring in Figure 9(a), with ring parameters $A = 100$km, $B = 0$ km, $y_c = 0$ km, $\alpha = \beta = 0$, and initial true anomaly $\nu_1 = 0^\circ$ (cyan), $\nu_2 = 90^\circ$ (blue), $\nu_3 = 180^\circ$ (green), $\nu_4 = -90^\circ$ (red). Each daughter as an initial mass $m_0 = 12$ kg, and a finite thrust engine of $T = 1$ N and $I_{sp} = 200$ s, with in plane thrust set to $k_1 = 1.0$, and out-of-plane thrust set to $k_2 = 0.5$. For each spacecraft on a ring, the maneuver for reconfiguration happens at the same location in the relative orbit, which ensures all spacecraft reconfigure to the same ring. In this case, the first reconfiguration occurs when each daughter reaches $\nu(t_1) = -90^\circ$. This means that the reconfiguration does not happen at the same time for each spacecraft. It takes about one orbit revolution to reconfigure all the spacecraft

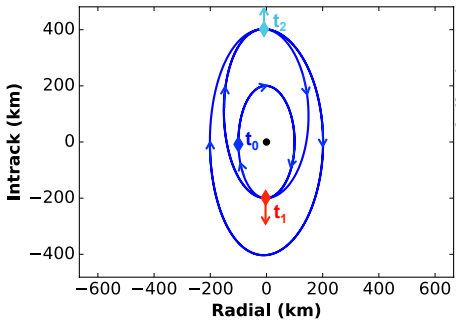

Figure 8. Spacecraft reconfiguration schematic by thrusting perpendicular to the velocity

on one ring. The second reconfiguration occurs once the daughters reach $\nu(t_2) = 90°$. The final location of the daughters is shown in the largest ring in Figure 9(a). Even though all spacecraft follow the same path in the relative, rotating frame of the mothership, in an inertial frame fixed at the Moon, the orbits are different, as can be seen by the orbital elements in Figure 9(b).

For a constellation with several rings of different sizes, the reconfiguration is designed to happen sequentially from largest to smallest ring to avoid any possible collisions. The spacecraft can reconfigure as many times as needed, within a given ΔV budget.

Stationkeeping Maneuvers

The design methods provided assume two-body dynamics and, therefore, when adding external perturbations, such as solar radiation pressure, drag, or the gravity of other planets and moons, the reference orbits will drift, causing the necessity of stationkeeping maneuvers. Two contour plots are shown in Figure 10, that represent the required ΔV to get back onto the reference path of a single daughter spacecraft orbiting the Moon, with ring parameters defined in Table 7. Both the x and y axis vary over a 24 hour period, where the y-axis is the maneuver time and the x-axis the target time. In figure (a), the daughter's orbit was designed assuming the mothership orbits at $5,000$ km, in a perfectly circular equatorial orbit. When adding the gravity of the Sun and Earth, the two most prominent gravity sources when orbiting the Moon, both the mother and daughter spacecraft deviate from their reference path, adding high ΔV costs to bring it back to the reference. However, the same *relative* motion of the daughter can be maintained with respect to the mothership, while allowing the mothership orbit to vary with the perturbing dynamics. In this case, the stationkeeping costs are greatly reduced, as is shown in figure (b). It is optimal in terms of time and ΔV to maneuver 2 hours after the previous target time, and target to a position state 22 hours later, the region encircled by the red square in Figure 10(b).

LUNAR RADIO INTERFEROMETER MISSION SCENARIO

Combining the methods discussed in the paper, a constellation mission scenario to observe distant galaxies is addressed, with 32 daughter spacecraft and a mothership in a circular, $5,000$ km orbit about the Moon. The mothership orbit was chosen for science purposes to be far enough from the Earth to avoid interference, as well as minimize gravitational perturbations from Earth. The maximum allowed baseline between any two spacecraft for science is 600 km. The design chosen is four rings, with 8 daughters in each ring. Each daughter weighs 12 kg, and has a 1 N thruster,

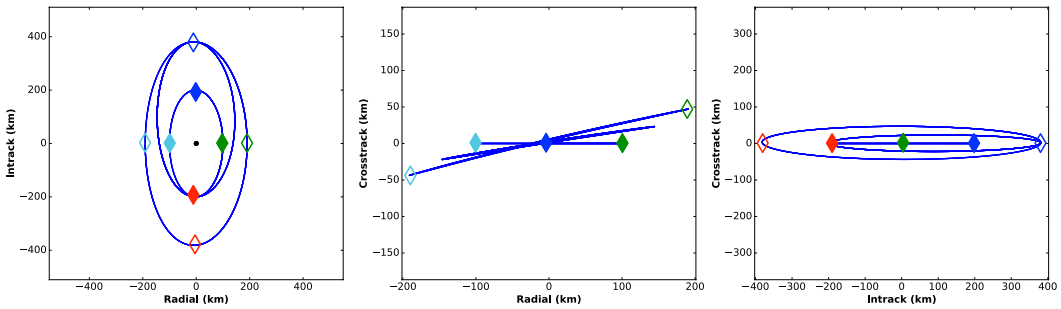

(a) Trajectory in radial, intrack, and crosstrack directions

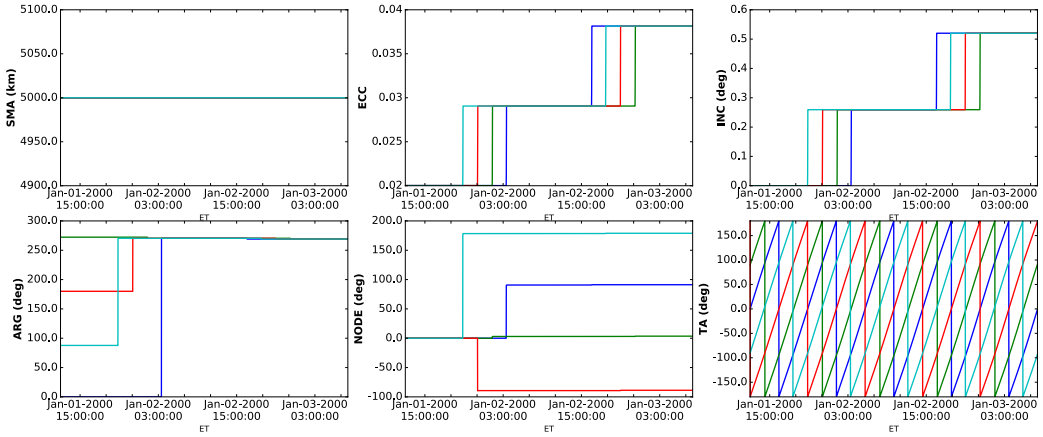

(b) Orbital elements over time

Figure 9. Four spacecraft on the same initial ring reconfigure to a larger ring size while maintaining constant period. The painted diamonds is each daughter at t_0, whereas the hollow diamonds are at the time the reconfiguration is finished.

with $Isp = 200$ s. The daughters deploy from the mothership spacecraft sequentially to their initial configuration shown in Figure 11(a) with parameters shown in Table 8, where inclination is defined as a function of the CLD parameters, inc $= \tan^{-1}(B/A)$. The mothership is at the center of the formation, shown in red. The deployment of each spacecraft to their initial configuration has been designed to cost 20 m/s for each daughter. After all the science data has been gathered and downlinked to Earth within a specific configuration, the daughters reconfigure, applying 1 m/s perpendicular to their velocity, which allows for 5 km increase in ring size. A total of 20 reconfigurations (equivalent to 20 m/s of propellant) are applied, ending in the final configuration shown in Figure 11(b) with parameters in Table 8. Using the stationkeeping design shown previously in Figure 10(b), this design strategy requires maneuvering once per day, which is achievable from an operational point of view. Over an entire month, the average ΔV/day is 0.27 m/s, with a maximum excursion of 0.55 m/s and minimum of 0.1 m/s.

Coverage and Baseline Computations

The formation design is driven by adequate coverage of collection targets, with coverage defined by the diversity of baselines formed by individual spacecraft pairs. A single baseline is the projec-

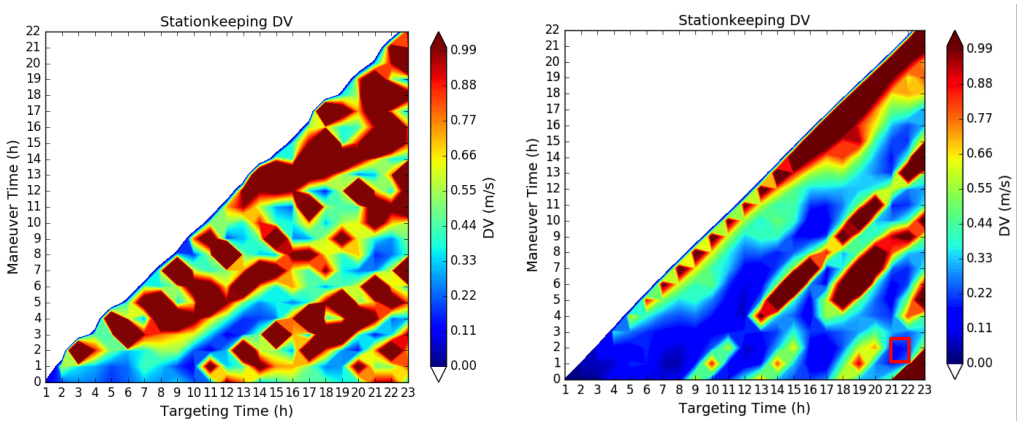

(a) ΔV for reference in two-body dynamics (b) ΔV for reference in full gravitational dynamics

Figure 10. Stationkeeping costs including Sun and Earth gravity for a daughter spacecraft in a low lunar orbit.

Table 8. Initial and Final Orbit Sizes with Respect to the Mothership of Each Ring

		Initial Configuration		Final Configuration	
Ring	Color (Fig. 11)	A (km)	inc. (deg)	A (km)	inc. (deg)
1	purple	200	0.0	400	0.0
2	green	160	25.5	300	18.5
3	blue	140	150.0	200	138.0
4	cyan	100	45.0	100	63.5

tion of the relative position vector from one spacecraft to another, into the plane perpendicular to the direction to a target. Baselines are computed beginning with the relative position vector from one spacecraft to another, $\vec{\rho}_{ij}$, and the unit vector to a target, $\hat{e}_\star$. Both vectors are assumed to be in a common inertial frame, EME2000 for this study. First, a new frame for projecting the position vectors is formed using the target vector and the z-axis unit vector in the EME2000 frame, where $\hat{e}_z = \hat{e}_\star$, $\hat{e}_y = \hat{k} \times \hat{e}_z$, $\hat{e}_x = \hat{e}_y \times \hat{e}_z$. where $\hat{e}_x$, $\hat{e}_y$, and $\hat{e}_z$ are the unit vectors defining the target frame; and $\hat{k}$ is the unit vector in the EME2000 z direction. For targets near 90° declination, the EME2000 x direction can be used in place of the z direction. With this target frame constructed each position vector $\vec{\rho}_{ij}$ is projected into the xy-plane of the target frame to yield (r, θ) pairs describing the baseline:

$$r = \sqrt{b_x^2 + b_y^2}$$
$$\theta = \tan^{-1}(b_y/b_x)$$

where b_x and b_y are the components of $\vec{\rho}_{ij}$ in the x and y directions of the target frame, respectively ($b_x = \vec{\rho}_{ij} \cdot \hat{e}_x$ and $b_y = \vec{\rho}_{ij} \cdot \hat{e}_y$). When computing baselines it does not make a difference if the baseline is measured from spacecraft i to spacecraft j, or vice-versa. Because of this a baseline of (r, θ) counts the same as one in the opposite direction, $(r, \theta + 180^\circ)$, and a formation of N spacecraft will have $N(N-1)/2$ unique baselines at a given sample time. For the purpose of computing coverage the (r, θ) space is divided up into n bins in the r direction and m bins spanning 180° in the θ direction, and credit is taken for each bin covered by a baseline. As the formation

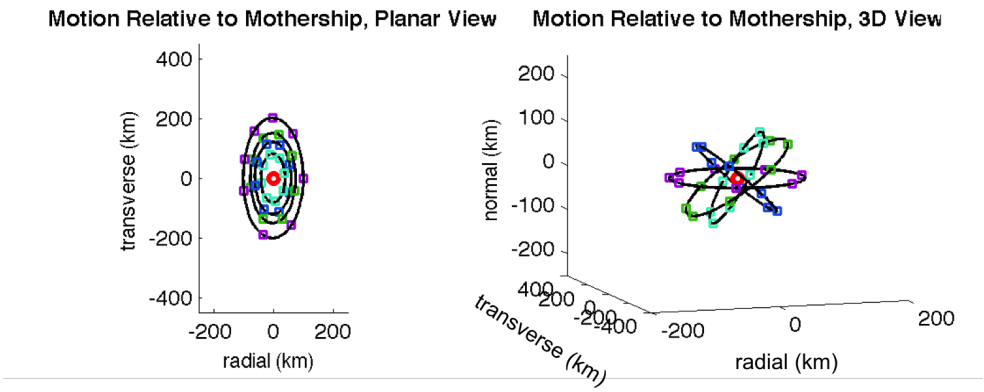

(a) Initial Configuration

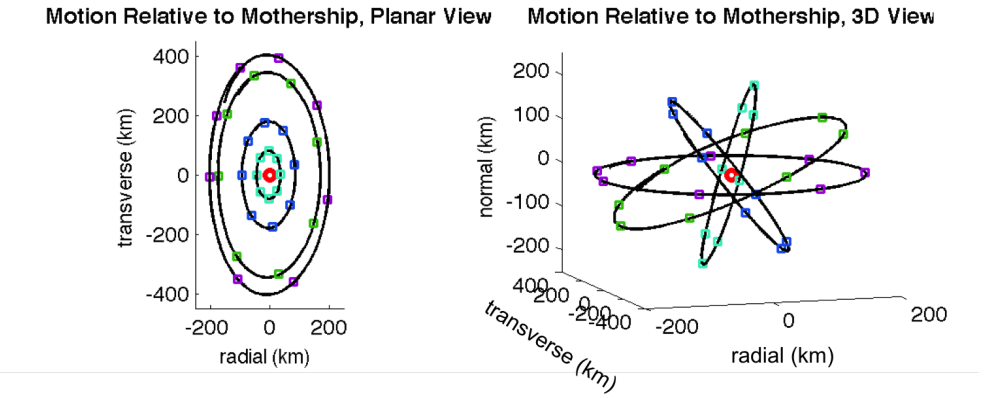

(b) Final Configuration

Figure 11. Daughtership Configurations in a Relative, Rotating Frame Fixed at the Mothership

geometry changes, new baseline measurements are taken, and the overall coverage consists of the different (r, θ) bins which have been collected. If n_{collect} is the number of bins collected over some period of time then a numerical coverage score, J, can be computed from $J = n_{\text{collect}}/(nm)$.

Figure 12 show baselines for the formation in the initial configuration in Table 8 against a targets with right ascension of 0° and declination of 45°. The figures use 128 bins in the radial direction and 128 bins to cover 180° in θ, with gridlines every 8 bins. Red bins indicate the instantaneous baselines at the time given while blue bins show bins already collected, with samples taken every 10 minutes. Since the formation reference orbit lies in the EME2000 xy-plane the cumulative baseline pattern will be flatter against targets with low declinations. In contrast, the pattern will be more round against targets with high declinations. Once the final configuration is achieved, the coverage pattern will cover a greater area of the baseline plot.

CONCLUSION

Two different methods for constellation design are presented: 1) Constellation design using Linear Dynamics (CLD) and 2) Constellation design using Invariant Manifold theory (CIM). The main

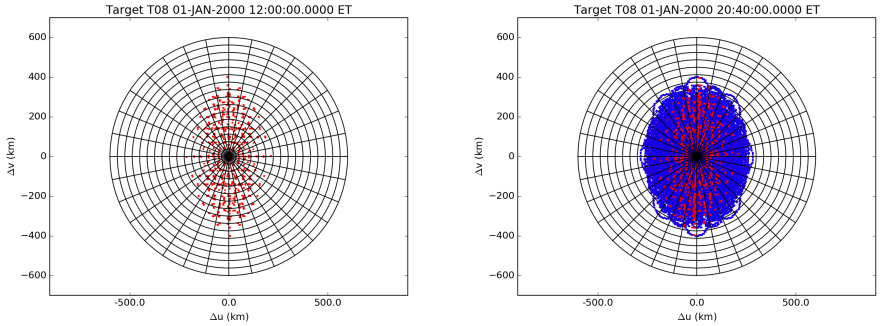

(a) Instantaneous for Initial Configuration (b) Cumulative One Orbit for Initial Conf.

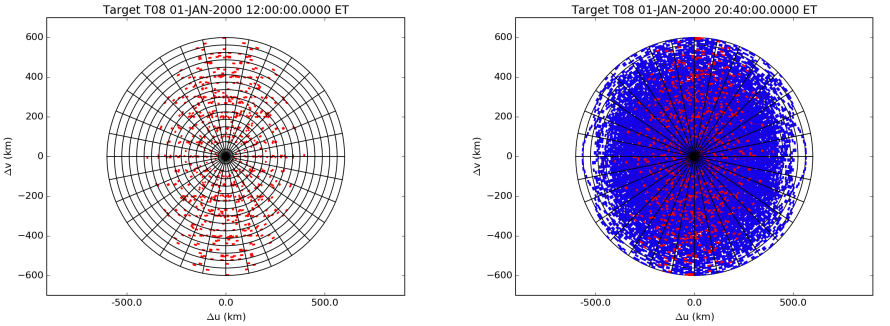

(c) Instantaneous for Final Configuration (d) Cumulative One Orbit for Final Conf.

Figure 12. Baselines for a Target at $(0°, 45°)$

design constraint for close-proximity constellations is that the period of their orbits be the same for all spacecraft. CLD uses the (linear) Clohessy-Wiltshire equations of motion. This method provides an analytical framework for fast and simple constellation design, which proves useful in the early design stages of a mission. Because this model assumes linear motion, conversion into nonlinear (more realistic) dynamics is important. We show that when converting to nonlinear dynamics, the shape of the linear relative motion can be maintained by fixing the semi-major axis of the conic orbit to that of the reference trajectory, and making the conversion at apogee of the relative orbit. CIM on the other hand uses invariant manifold theory, exciting the center eigenvalues for the constellation design. However, both methods require $5N$ parameters to fully define a constellation, where N is the total number of spacecraft. Even though both methods are derived using completely different approaches, the fact that they require the same number of parameters to define the constellation, leads to believe that they are mathematically equivalent. This yet remains to be rigorously proven. The main advantage of CIM is that the design is not restricted to linear or two-body dynamics. The method makes use of the state transition matrix, which can be computed numerically for any unique type of environment. The main disadvantage of this method is that, for simple dynamical environments, the computation of the constellation is slower than when using CLD.

We make use of the aforementioned constellation design methods to build two mission scenarios, both with a radio interferometer science objective. The first example is a six spacecraft constellation in a GEO graveyard orbit, where the constellation is passively maintained at a maximum baseline

distance of 15 km. The second example is a thirty-two spacecraft constellation orbiting the Moon with a period of 8.8 hours, with a maximum baseline distance of 600 km. For the latter mission, allowing for reconfiguration of the constellation is crucial for obtaining maximum science data. The period of the constellation needs to stay constant, and therefore, reconfiguration is performed by thrusting perpendicular to the velocity. The design strategy is valid for both high and low-thrust engines. Deployment and stationkeeping maneuver strategies are also outlined in the paper.

Future work will focus on designing constellations in more complex dynamics, such as the restricted three body problem or higher-order dynamics, in which gravity of other planets, solar radiation pressure, and drag are considered in the initial design process, therefore reducing the need for constant stationkeeping maneuvers. Transportation of the constellation from one location to the other while actively maintaining the constellation geometry will also be studied.

ACKNOWLEDGMENT

This research was carried out at the Jet Propulsion Laboratory, California Institute of Technology, under a contract with the National Aeronautics and Space Administration.

© 2017. California Institute of Technology. Government sponsorship acknowledged.

REFERENCES

[1] S. Conford *et al.*, "Evaluating a fractionated spacecraft system: A business case tool for darpa's f6 program," *IEEE Aerospace Conference*, 2012, pp. 1–20.

[2] S. Schaffer, S. Chien, A. Branch, and S. Hernandez, "Preliminary Results on Heuristic-Guided Orbit Selection for a Radio-Interferometric Spacecraft Constellation," *In Proc. Workshop on AI in the Oceans and Space, International Joint Conf. on Artificial Intelligence*, Aug. 2017.

[3] J. Stuart, A. Dorsey, F. Alibay, and N. Felipe, "Formation Flying and Position Determination for a Space-Based Interferometer in GEO Graveyard Orbit," *IEEE Aerospace Conference*, 2017. DOI: 10.1109/AERO.2017.7943705.

[4] K. Belov *et al.*, "A Space-based Decametric Wavelength Radio Telescope Concept," *Experimental Astonomy*. Submitted.

[5] W. H. Clohessy and R. S. Wiltshire, "Terminal Guidance System for Satellite Rendezvous," *Journal of the Aerospace Sciences*, Vol. 27, No. 9, 1960, pp. 653–658.

[6] J. E. Prussing and B. A. Conway, *Orbital Mechanics*. No. Ch. 8, Oxford University Press, 1993.

[7] I. Hussein and A. Block, "Dynamic Coverage Optimal Control for Interferometric Imaging Spacecraft Formations," 2004.

[8] I. Hussein, D. Scheeres, and D. Hyland, "Optimal Formation Control for Imaging and Fuel Usage," 2005. AAS 05-160.

[9] L. Millard and K. Howell, "Control of Interferometric Spacecraft Arrays for (u,v) Plane Coverage in Multi-Body Regimes," *Journal of the Astronautical Sciences*, Vol. 56, No. 1, 2008.

[10] J. Kennedy and R. C. Eberhart, "Particle Swarm Optimization," *Proceedings of the IEEE Conference on Neural Networks*, Nov.-Dec. 1995, pp. 1942–1948.

[11] C. Roscoe, S. Vadali, K. Alfriend, and U. Desai, "Optimal Formation Design for Magnetospheric Multiscale Mission Using Differential Orbital Elements," *Journal of Guidance, Control, and Dynamics*, Vol. 34, No. 4, 2011, pp. 1070–1080. DOI: 10.2514/1.52484.

[12] K. Alfriend, S. Vadali, P. Gurfil, J. How, and L. Barger, *Spacecraft Formation Flying: Dynamics, Control, and Navigation*. Elsevier, 2010.

[13] B. Barden and K. Howell, "Fundamental Motions near Collinear Libration Points and Their Transitions," *Journal of the Astronautical Sciences*, Vol. 46, No. 4, 1998, pp. 361–378.

[14] H. D. Curtis, *Orbital Mechanics for Engineering Students*, pp. 383–387. Oxford, UK: Elsevier, 2014.

[15] Z. Olikara and K. Howell, "Computation of Quasi-Periodic Invariant Tori in the Restricted Three-Body Problem," *Journal of the Astronautical Sciences*, Vol. 136, No. 1, 2010, pp. 313–327.